

Article

Indirect Prediction of Salt Affected Soil Indicator Properties through Habitat Types of a Natural Saline Grassland Using Unmanned Aerial Vehicle Imagery

László Pásztor, Katalin Takács *, János Mészáros , Gábor Szatmári , Mátyás Árvai , Tibor Tóth , Gyöngyi Barna , Sándor Koós, Zsófia Adrienn Kovács, Péter László and Kitti Balog 

Institute for Soil Sciences, Centre for Agricultural Research, Herman Ottó Rd. 15., H-1022 Budapest, Hungary; pasztor.laszlo@atk.hu (L.P.); meszaros.janos@atk.hu (J.M.); szatmari.gabor@atk.hu (G.S.); arvai.matyas@atk.hu (M.Á.); toth.tibor@atk.hu (T.T.); barna.gyongyi@atk.hu (G.B.); koos.sandor@atk.hu (S.K.); kovacs.zsofia@atk.hu (Z.A.K.); laszlo.peter@atk.hu (P.L.); balog.kitti@atk.hu (K.B.)

* Correspondence: takacs.katalin@rissac.hu

Abstract: Salt meadows, protected within National Parks, cannot be directly surveyed, yet understanding their soil condition is crucial. Our study indirectly estimates soil parameters (Total Salt Content (TSC), Na, and pH) related to salinization/sodification/alkalinization using spectral indices and UAV survey-derived elevation model, focusing on continental lowland salt meadows. A vegetation map was created using 16 spectral indices and a Digital Elevation Model calculated from RGB orthophotos using photogrammetry. Field observations helped define habitat types based on the General National Habitat Classification System (Hungary), and quadrats with complete coverage of specific plant species were identified. Machine learning was employed on 84 training quadrats to develop a prediction algorithm for vegetation patterns. Five saline habitat types, representing variations in soil properties and topography, were identified. Spectral and topomorphometric indices derived from UAV were key to the spatial prediction of soil properties, employing random forest and co-kriging methods. TSC, Na, and pH data served as indicators of salt-affected soils (SAS), and thematic maps were generated for each indicator (57 samples). Overlapping with the vegetation map, the probability range of estimated SAS indicator values was determined. Consequently, a model-based estimation of soil pH, TSC, and Na conditions is provided for habitat types without disturbing protected areas.

Keywords: protected salt meadows; vegetation map; machine learning methods; UAV; spectral indices; SAS indicator prediction



Citation: Pásztor, L.; Takács, K.; Mészáros, J.; Szatmári, G.; Árvai, M.; Tóth, T.; Barna, G.; Koós, S.; Kovács, Z.A.; László, P.; et al. Indirect Prediction of Salt Affected Soil Indicator Properties through Habitat Types of a Natural Saline Grassland Using Unmanned Aerial Vehicle Imagery. *Land* **2023**, *12*, 1516. <https://doi.org/10.3390/land12081516>

Academic Editors: Tiago Brito Ramos, Maria da Conceição Gonçalves and Mohammad Farzaman

Received: 30 June 2023
Revised: 21 July 2023
Accepted: 25 July 2023
Published: 30 July 2023



Copyright: © 2023 by the authors. Licensee MDPI, Basel, Switzerland. This article is an open access article distributed under the terms and conditions of the Creative Commons Attribution (CC BY) license (<https://creativecommons.org/licenses/by/4.0/>).

1. Introduction

Natural semi-arid saline steppes and salt marshes, which are mostly protected as part of National Parks, are ecologically valuable ecosystems that play a crucial role in maintaining biodiversity and providing various ecosystem services [1–3]. Preserving these habitats is of high importance in the European Union ([4], Natura 2000 network of protected areas) [5]. However, due to their protected status, direct surveys such as disturbance of surface of these areas with excavations are often restricted, making it challenging to assess their soil condition. As a consequence of the current variable climatic conditions, the hydrological and soil formation conditions are also changing [6], thus understanding and monitoring the soil parameters related to salinization [7], sodification, and alkalinization is essential for effective management and conservation of these sensitive habitats.

Digital soil mapping (DSM, [8]) has emerged as a valuable tool providing spatial soil information across a wide range of soil-related applications [9], including precision agriculture, hydrology, environmental sciences, conservation biology, or spatial planning [10]. DSM approach offers an alternative to conventional mapping methods for the spatial

assessment of soil properties such as soil salinity [11,12]. In DSM, a wide range of spatial data is collected, integrated, and analyzed using geostatistical methods and/or machine learning techniques for inferring the spatial variability of soil characteristics [13–16].

Remote sensing provides a wealth of information about land surface, with improving spatial, temporal, and spectral resolutions, which can be used in assessing the spatial variability of soil properties in different ways. (i) Bare surface soil characteristics can be directly obtained by remote sensing. Spectral reflectance features in the visible, near-infrared, and shortwave infrared spectrum can be used as a direct indicator for soil surface salinity [12,17]. Increased reflectance can be observed particularly in the blue band [18,19]. Surface soil salinity does not necessarily reflect actual salinity levels of the whole profile [20], but (ii) indirect information about subsurface salinity conditions can be gathered through vegetation type and plant growth as these are controlled by root zone soil properties [17]. (iii) Remote sensing based environmental covariates such as digital elevation models (DEM) and its derivatives (e.g., slope, aspect, and topographic wetness index), spectral band data, vegetation indices, land use, and land cover maps are proved to be useful in DSM for characterizing the most relevant environmental variables representing the soil forming factors [18,21].

Remote sensing is also a valuable, fast, and non-destructive tool to overcome the limitations of direct surveys for monitoring and assessing inaccessible areas such as wetlands [22,23] or protected areas [24]. In recent years, the application of aerial surveys using Unmanned Aerial Vehicles (UAVs) has shown great potential in the spatial assessment of a wide range of features in agriculture and soil science such as vegetation patterns [25,26], monitoring invasive plants [27], peat soil properties [28], soil erosion mapping [29], soil productivity [30], or soil water content mapping [31]. UAV-based data applications have shown their utility also in improving accuracy and providing more insights into soil salinity mapping [19,20,32,33].

In this study, we aim to indirectly estimate soil parameters, specifically Total Salt Content (TSC) [34], sodium (Na) concentration, and pH, by utilizing spectral indices calculated from RGB sensor based orthomosaic and DEM.

The database was derived from aerial surveys in Europe's largest continuous natural semi-arid steppe (in total 82,000 ha, of which 100 ha area was studied) in Hortobágy (Hortobágy National Park) which is a special part of the Great Hungarian Plain. According to our concept, distinct saline habitat types (vegetation patches) differentiated based on various vegetation colors, can be determined using spectral indices derived from orthophotos captured in the visible spectrum (RGB) [35]. As halophytic plant communities exhibit distinct elevation zones ranging from wet salt meadows to dry closed steppes [36,37], surface elevation plays a critical role [38]. Therefore, in our study, we utilized DEMs in conjunction with spectral indices [39] for vegetation mapping on the test area. This article describes the altitude-based distribution of saline habitats and estimates pH, TSC, and Na concentration value categories using a model constructed based on field-validated points for the distinct habitat types. The applied predictive model employing machine learning methods, namely random forest combined with kriging [40–42] was developed, to provide a reliable estimation of these salt affected soil indicator properties, namely pH, TSC, and Na concentration. Thus, indirect estimation of soil properties using remote sensing data and machine learning techniques has significant implications for the monitoring, management and conservation of these ecologically important habitats. The findings of this study will contribute to a better understanding of the soil condition in salt meadows, despite their protected status.

2. Materials and Methods

2.1. Study Site

The study site is a protected salt marsh, which is a part of the largest contiguous natural saline grassland area in Europe, located in the Eastern region of Hungary, in Hortobágy National Park (Hortobágy NP) (Figure 1). The sampling plot has a rectangular

shape (corner coordinates of 47°22′10.67″ N 21°04′27.02″ E; 47°22′39.83″ N 21°04′28.14″ E; 47°22′39.08″ N 21°05′10.98″ E; 47°22′09.91″ N; 21°05′09.86″ E) fitting to a 1 km² grid in the Hungarian National Grid System (EOV/HD72—EPSG:23700) and belongs to the Central Tisza Region, microregion of Hortobágy according to [43]. The sample area is a plain lying between 85.9 and 87.5 m a.m.s.l. and covered with fine-grained sediments (clay, silt) [44]. Despite the relatively low relief, the area is rich in pedological and geomorphologic features [45]. The River Tisza has deposited silt into the loess-silt surface depressions, which had salinization/sodification process with various types of salts, including NaHCO₃, NaCl, Na₂SO₄, and MgSO₄, as documented by [46,47]. The area is characterized by deep saline, sodic soils, which make up a mosaic spatial structure with diverse saline soil complexes. Largest area is dominated by *Meadow solonetz* {Hungarian official nomenclature} soils (Solonetz according to [48]) with a clay loam texture utilized as saline pastures. Smaller areas are covered with *Steppe meadow solonetz* (Chernozems or Solonetz according to [48]) soil and *Solonetzic meadow* soils (Gleysol or Vertisol according to [48]) as well [43,49]. Groundwater level is between 2 and 4 m, chemically rich in sodium [46,47], which has contributed to the salinization of the soil in the sample area. Salt- and drought-tolerant plant communities live on these salt affected soils and the flora of the landscape is also extremely diverse. Even a decimeter difference in surface elevation also results in a different vegetation pattern, which is closely related to changes in soil salinity and moisture content [50,51]. The microregion of the study area has moderately warm, dry climate; the value of aridity index is 1.30–1.35. The annual precipitation average ranges from 510 to 550 mm with high temporal and spatial variability. Total annual solar radiation ranges between 1900–1940 h, whereas long-term mean annual temperature is 10.0–10.2 °C [43]. Although networked by many channels, the area has a negative water balance.

Summarizing the sedimentological, pedological, climatic and water-holding conditions of the sample area, it can be stated that this area presents a very diverse, mosaic picture, where the vegetation zones on saline soils reflect the spatial variation in soil salinity and moisture in correlation with the surface elevation.

2.2. Field Survey and Laboratory Analysis

In order to capture small scale spatial heterogeneity of the salt and textural pattern of the study site, both in situ field measurements and ex situ laboratory measurements were implemented during the research. In situ measurements included vegetation survey. Aerial assessment was conducted to collect imagery information by using UAV. These non-destructive methods can also be applied on soil surface of protected nature saline areas where invasive approaches are not permitted.

2.2.1. Soil Sampling

For taking undisturbed soil samples for further laboratory analysis, 100 sampling points were designated on the 1 km² sample area, in a 100 × 100 m regular grid. Due to accessibility problems in the waterlogged parts of the site, and the difficulty of drilling through impenetrable hard near-surface layers on other parts of the site, 57 of the planned 100 points were drilled (Figure 1b), with motorized hand drill down to 1 m depth. Undisturbed soil sample columns were collected in plastic tubes having 10 cm in diameter for further analysis. Beyond, at 0–30 cm depth, composite soil samples were also taken in April 2020. In addition, at 3 characteristic locations of the sample area, soil profiles were excavated for soil sampling and soil classification in July 2020. Ex situ laboratory measurements were carried out, and numerous soil parameters were determined. In this study, total salt content (TSC), reaction (pH), and Na concentration of the soil (Na)—as parameters related to salinization/sodification/alkalinization—were investigated as predictors for thematic mapping.

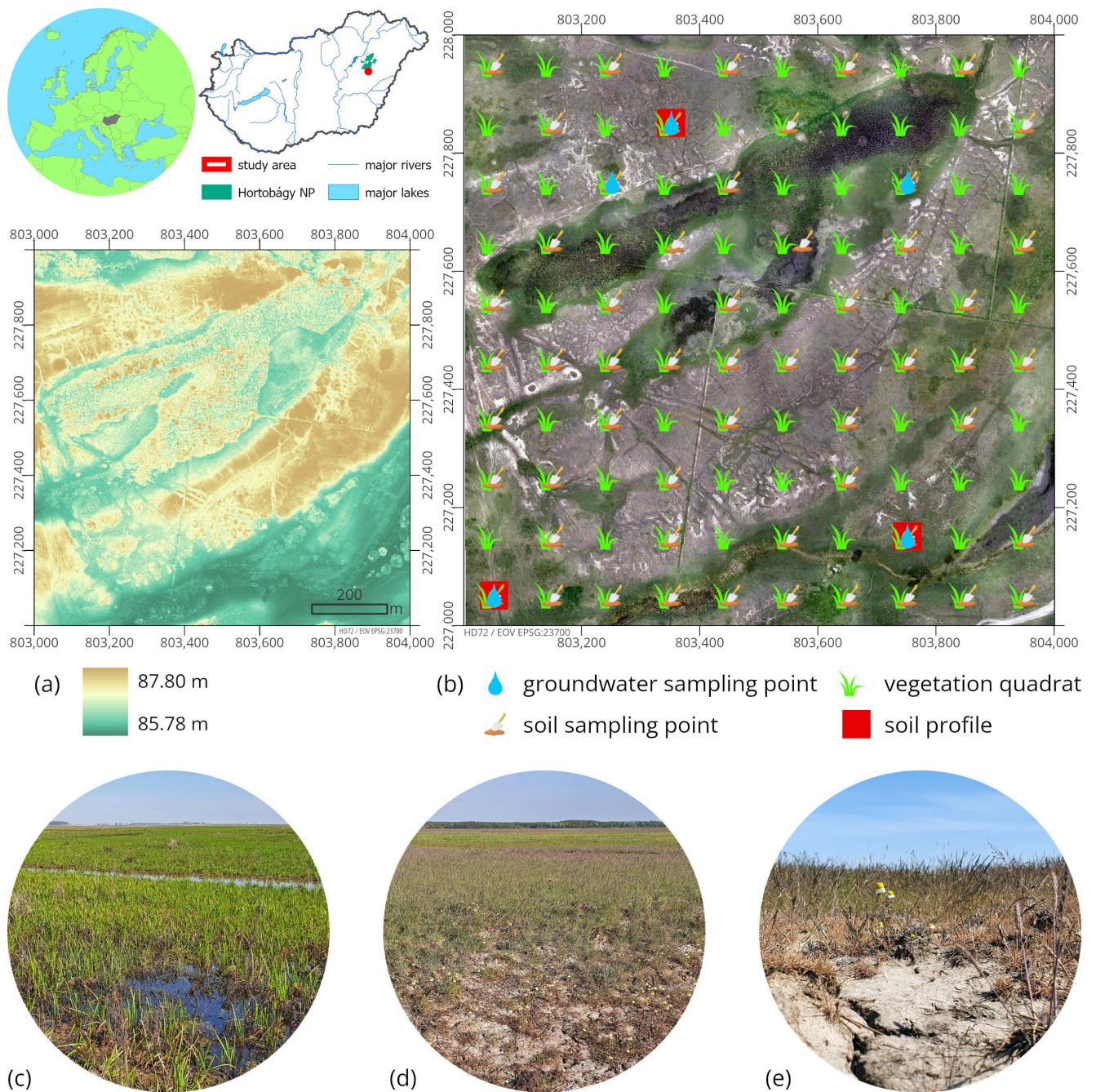


Figure 1. Location and characteristics of the study area. (a) Topography; (b) sampling sites on RGB orthomosaic background; (c) salt meadow; (d) transition of a bare spot (in the foreground) to Artemisia steppe (in the background); (e) bare spot with *Matricaria chamomilla* surrounded by *Puccinellia limosa* plants.

2.2.2. Vegetation Survey

The 1 km² sample area was divided into 1-hectare sections. Within each hectare, vegetation was assessed using the 10 × 10 m quadrat method. This resulted in 100 vegetation quadrats (Figure 1b), where the spatial percentage cover of each vegetation type within the quadrat was determined. The vegetation in each quadrat was then classified into habitat types according to the Hungarian General National Habitat Classification System (Á-NÉR; [52,53]), based on the occurring plant species ([52,53], Table 1).

Table 1. Habitat types present on the study area.

Habitat Code	Description of Habitat Type	Note
B6	Salt marshes	
F1b	Achillea steppes on <i>Meadow solonetz</i>	
F2	Salt meadows	
F5	Annual salt pioneer swards of steppes and lakes	<i>“padkásszik”</i> (microerosional mound)
F5bs ¹	Annual salt pioneer swards of steppes and lakes	<i>“vakszik”</i> (bare spot)
H5a	Closed steppes on loess	
U9	Standing waters	

¹ Added by the Authors, it is not part of the Á-NÉR system.

For habitat type F5, we have separated the *“vakszik”* (bare spot in vegetation of annual and perennial plants of usually small alkali mud surfaces) and the *“padkásszik”* (microerosional mound) types, because there is no surface height difference in the extent of the bare spot, while for the microerosional mound there can be a height difference of several cm, which can be an important difference for mapping. Therefore, the F5bs category was established solely for the bare spot in this study, and the genuine F5 was kept for the vegetation of microerosional mound habitat.

2.2.3. Proximal Soil Sensing

Aerial survey was conducted at the study site in April 2020, using UAV with a visible range (RGB) camera onboard. A 24 MP Fuji X-T20 camera was applied for the survey having an APS-C sensor; focal length of 14 mm; angle of view: 91°; automatic ISO speed; automated exposure time based on the sharpness, color saturation, and brightness of input images. Aerial survey was performed in a fully automatic flight mode with image overlap of 80% and sidelap of 60% for helping the proper photogrammetric processing. In terms of focal length and resolution, altitude of 120 m was found to be sufficient for recording and separating vegetation patches. Nine ground control points (GCP) were placed at the soil surface of the study site and were measured with a South Galaxy G1 type real-time kinematic correction GPS unit, having a nominal 1 cm horizontal and vertical accuracy. These GCPs were used to transform raw images into the Hungarian National coordinate system (EOV/HD72–EPSG:23700). During the photogrammetrical processing (orthorectification) of raw images, the RGB orthomosaic and DEM of the study area were generated. The whole workflow was performed in Agisoft Metashape Professional (Version 1.6.1). At the end, both datasets were transformed into the EOV/HD72 coordinate system and exported at 0.5 m spatial resolution.

As ancillary data, additional co-variable layers were calculated based on both datasets (RGB mosaic and DEM). With the help of the *“uavRst”* R package [54] 16 spectral indices were generated using the red, green, and blue bands of the mosaic. The different spectral indices can estimate different properties of vegetation and in some cases soil surface of salt affected soils, e.g., brightness index—bare spots, open water surfaces; redness index—biomass estimation and stand health. The combined use of the calculated spectral indices can help to complement multidimensional information and achieve more reliable results, thus increasing the accuracy of the vegetation map. Secondly, 20 topomorphometric layers were calculated using the SAGA GIS [55] Channels, Hydrology, and Morphometry libraries. The detailed description of all environmental co-variables can be found in Table 2.

Table 2. List of environmental co-variables used in vegetation mapping and spatial modelling of soil properties.

	Environmental Co-Variable	Reference
Spectral indices	Red band (R)	
	Green band (G)	
	Blue band (B)	
	Visible Vegetation Index (VVI)	[56]
	Visible Atmospherically Resistant Index (VARI)	[57]
	Normalized Difference Turbidity Index (NDTI)	[58]
	Redness Index (RI)	[59]
	Soil Color Index (SCI)	[60]
	Brightness Index (BI)	[61]
	Spectral Slope Saturation Index (SI)	[61]
	Hue Index (HI)	[61]
	Triangular Greenness Index (TGI)	[62]
	Green Leaf Index (GLI)	[63]
	Normalized Green Red Difference Index (NGRDI)	[64]
	Green Leaf Area Index (GLAI)	[54]
	Overall Hue Index (HUE)	[65]
	Coloration Index (CI)	[65]
Overall Saturation Index (SAT)	[65]	
Shape Index (SHP)	[65]	
Topomorphometric indices	DEM	
	Slope	[66]
	Aspect	[66]
	Topographic Position Index (TPI)	[67]
	Terrain Ruggedness Index (TRI)	[68]
	Surface roughness (SR)	[69]
	Flow direction (flowdir)	[70]
	Catchment area (carea)	[70]
	Modified catchment area (mcare)	[71]
	General curvature (GC)	[70]
	Diurnal anisotropic heating (DAH)	[72]
	LS factor (LS)	[73]
	Mass Balance Index (MBI)	[74]
	Multi-resolution Ridge Top Flatness (MRRTF)	[75]
	Multi-resolution Valley Bottom Flatness (MRVBF)	[75]
	Real Surface Area (RSA)	[66]
	Stream Power Index (SPI)	[73]
SAGA Wetness Index (SAGAWI)	[71]	
Vertical distance to channel network (vd2cn)	[66]	
Channel network base level (cnbl)	[66]	
Topographic Wetness Index (TWI)	[76]	

2.2.4. Laboratory Measurements

The collected groundwater samples were analyzed for pH and electrical conductivity (EC), furthermore, cation composition was measured according to the Hungarian standards (summarized in Table 3) in order to determine the sodium adsorption ratio (SAR).

pH and EC of groundwater were measured with Multi Line P4, WTW Multi 350i combined electrode and conductometer, respectively.

Reaction of groundwater was determined using direct potentiometry, following the Hungarian standard Nr. 1484-22:2009 (Table 3, Note 1).

Table 3. List of Hungarian standards of the measured groundwater and soil parameters.

Hungarian Standard of the Measurement	Parameter	Unit	Instrument	Accuracy	Nr. of Data
MSZ 1484-22:2009 (Note 1)	pH of groundwater	-	Multi Line P4, WTW Multi 350i, Xylem Analytics Germany Sales GmbH & Co. KG, WTW, Weilheim, Germany	0.004	5
MSZ EN 27888:1998 (Note2)	Electrical conductivity of groundwater	dS/m	Multi Line P4, WTW Multi 350i, Xylem Analytics Germany Sales GmbH & Co. KG, WTW, Weilheim, Germany	1 µS/cm	5
MSZ 1484-3:2006 (Note 3)	Calcium and Magnesium ion concentration of ground water	mg/L	Ultima-2 type ICP OES, Horiba Jobin Yvon SAS., Longjumeau, France	0.5 µg/L	5
MSZ 1484-3:2006 (Note 3)	Sodium and Potassium ion concentration of groundwater	mg/L	Ultima-2 type ICP OES, Horiba Jobin Yvon SAS, Longjumeau, France Radelkis OP-300, Radelkis Elektroanalitikai Műszergyártó	0.5 (Mg), 1.0 (Na) µg/L	5
MSZ-08-0206-2:1978, 2.1 section (Note 4)	Reaction of the soil	pH	Kft, Budapest, Hungary, digital pH measuring device, Sentron Europe B.V., Leek, The Netherlands	±0.05	57
MSZ-08-0206-2:1978, 2.4 section (Note 4)	Total salt content of soil	w/w%	Radelkis OK-102/1 conductometer, Radelkis Elektroanalitikai Műszergyártó Kft, Budapest, Hungary iCAP 7400 ICP-OES Analyzer Thermo Scientific Duo View,	5–7.5 rel.%	57
MSZ 20135:1999, 5.1 (Note 5)	Na concentration of soil	mg/kg	Thermo Fisher Scientific (Praha) s.r.o., Praha, Czech republic	4–7.5 rel.%	57

The laboratory measurement data are the results of averaging three parallel measurements. Note 1: "Water quality. Part 22: Determination of pH and pH in equilibrium state." MSZ 1484-22:2009. 2009. (in Hungarian); Note 2: "Water quality. Determination of electrical conductivity" MSZ EN 27888:1998 (ISO 7888:1985). 1998 (in Hungarian); Note 3: "Testing of waters, Part 3: Determination of dissolved, suspended and total metals in water by AAS and ICP-OES" MSZ 1484-3:2006. 2006 (in Hungarian); Note 4: "Evaluation of some chemical properties of the soil. Laboratory tests (pH value, phenolphthaleine alkalinity expressed in soda, all water soluble salts, hydrolite /y1 value/ and exchanging acidity /y2-value/" MSZ-08-0206-2:1978. 1978 (in Hungarian), Note 5: "Determination of the soluble nutrient element content of the soil" MSZ 20135:1999. 1999 (in Hungarian), The Hungarian standards are available via the following website: <http://szabvanykonyvtar.msz.hu/> (accessed on 29 June 2023).

Direct potentiometry relies on measuring the potential on the surface of an electrode submerged in an electrolyte solution. This potential is measured by calculating the voltage difference between the measuring electrode (glass electrode) and the reference electrode (e.g., Ag/AgCl). The glass electrode surface has a well-defined potential relative to the surrounding aqueous solution, which is linearly related to the pH of the solution. A combined electrode was used for pH measurement, integrating both the measuring and reference electrodes. This electrode consists of a double-walled glass tube containing a buffer solution inside and the reference electrode outside. Essentially, the electrode acts as a membrane that, upon contact with an aqueous solution, absorbs water and swells, establishing an ion exchange equilibrium with the solution's protons to be measured. The potential across the membrane is determined by the concentration ratio of H⁺ ions on each

side. The buffer solution inside the glass sphere ensures a constant concentration of H^+ , allowing the electrode potential to depend solely on the external H^+ concentration, which is directly proportional to the pH of the solution.

Hungarian standard No. 27888:1998 (Table 3, Note 2) was used for determining water quality, specifically providing guidelines for measuring the electrical conductivity of water. The standard is fully aligned with the European standard EN 27888:1993. Electric conductivity measures the water's ability to conduct electricity, which is determined by the quantity and quality of water-soluble salts present. A higher conductivity value indicates a higher concentration of dissolved salts in the water. The conductometric measurement methodology is based on determining the resistance (electrical resistivity) of the solution between two electrodes, either flat or cylindrical, separated by a fixed distance. Electrical conductivity can be calculated as the reciprocal of electrical resistivity.

Hungarian standard No. 1484-3:2006 (Table 3, Note 3) specifies the possibility of measuring the dissolved Ca, Mg, Na, and K content of groundwater—among other elements—by inductively coupled plasma optical emission spectroscopy (ICP-OES). ICP-OES allowing the simultaneous detection and a sensitive, accurate quantification of 70–80 different elements.

The collected groundwater samples were filtered through a 0.45 μm pore mesh membrane filter. Then, it was sprayed inside the equipment, using argon as carrier gas. The components of the sample evaporate at a temperature of 6000 K inside the chamber, atomize, the resulting free atoms are excited. The excited atoms, as they transition to a lower energy level, emitting photons at wavelengths characteristic of the given element. We spectrally resolve the plasma light emission and measure the intensity of each element in a specific wavelength spectral line using detectors. The quantities of the investigated elements (Ca, Mg, Na, and K) are determined through calibration using a series of solutions with known element concentrations.

SAR is a water quality parameter used in soil science to express sodicity hazard of ground water by showing the relative activity of sodium ions in the exchange reactions with the soil relative to calcium and magnesium. SAR value was calculated according to Equation (1):

$$\text{SAR} = \frac{\text{Na}^+}{\sqrt{\frac{1}{2}(\text{Ca}^{2+} + \text{Mg}^{2+})}} \quad (1)$$

where Na, Ca, and Mg are ion concentrations all displayed in meq/L.

SAR is widely used in the irrigation management of sodium-affected soils, and have to be assessed combined with EC, according to the interpretive guidelines of [77].

Soil chemical analysis was conducted on composite soil samples from the experimental site, from the depth of 0–30 cm. In the laboratory, pH, TSC, and Na concentration was measured according to the actual Hungarian standards (see Table 3).

pH was measured from 1:2.5 proportioned (6 g soil: 15 mL n KCl) suspension with Radelkis OP-300 digital pH-meter, using potentiometry method according to Hungarian standard No. 08-0206-2:1978, 2.1 section (Table 3, Note 4). The pH measurement is conducted using a procedure similar to that used for groundwater analysis, with the exception that the chemistry of a soil suspension is evaluated. To ensure accurate results, it is necessary to allow a minimum of 12 h for the ionic balance of the soil suspension to stabilize before the measurement is taken. It is important to note that the suspension should not be filtered prior to the pH assessment.

To determine the Total Salt Content (TSC), soil paste saturated with water up to its plasticity limit was used. The measurements were conducted using the Radelkis OK-102/1 conductometer, following the guidelines of Hungarian standard No. 08-0206-2:1978, 2.2.4 section (Table 3, Note 4). A known-capacity immersion electrode was carefully inserted into the soil paste. The resistance of the soil paste was measured, allowing the device to calculate the specific conductivity and the total salt content (%) based on the provided

calibration table. The verification of electrode capacity was carried out using known concentration KCl solutions.

The determination of the soluble nutrient content of soil, including the measurement of sodium (Na) concentration available for plant uptake, is described in Hungarian standard No. 20135:1999 (Table 3, Note 5). In this method, the Na concentration in the soil was extracted using a solution of ammonium-lactate (AL) in a soil-to-solution ratio of 1:20. The extract was then filtered, and the Na concentration was determined using an ICP OES instrument, specifically the Thermo Scientific iCAP 7400 Duo View type.

2.3. Methods

2.3.1. Vegetation Mapping

Based on the environmental co-variable dataset, the classification of the sample area was performed using the habitat type survey as training areas, where the same habitat type covered the whole quadrat. Unfortunately, there was no information about the actual spatial coverage of the different habitat types present inside the polygon for quadrats with mixed habitats, only their ratio, therefore they were removed from the dataset. Artificial quadrats of classes standing water (3) and bare spot (9) were added manually in the same spatial size as the habitat quadrats (10 × 10 m). In total 72 field and 12 additional quadrats were used as training areas.

Values of pixels falling under the quadrat polygons from all spectral and topographic layers were extracted (33,600 data points), later used as training and testing data (divided in 70/30 ratio in a balanced way regarding the number of pixels of each class present in the study area) for the classification. Class separability analysis was performed using the extracted data showing water as a completely separate category, bare spot as a slightly overlapping class with all other vegetation related categories. Latter ones have major overlaps to each other in general; however, they can be separated based on their average heights in the DEM and using the topomorphometric layers as well. The “ranger” machine learning R package (v0.15.1 [78]) was used to build up a random forest based classifier, the hyperparameters were optimized with the help of the “caret” package (v6.0-94 [79]) to find the optimal set, where `min.node.size` was held constant at a value of 1 and two other parameters (`mtry` and `splitrule`) were 40 and `extratrees`, respectively. Any other hyperparameter was defined on their default values. At the end, the raster dataset containing all mentioned environmental co-variables in layers was classified with the trained model.

For any further analysis, this map was considered as the vegetation and habitat type map of the study site.

2.3.2. Spatial Modelling of Soil Properties

A hybrid machine learning and geostatistical approach was used for topsoil (0–30 cm) property estimations. In DSM random forest combined with kriging (RFK) is considered to be a new “workhorse” [13]. In this case, at first the spatial variation in soil properties was modelled with random forest (RF, [80]) based on the environmental covariates, which were generated from the DEM and RGB orthophoto (Table 2). RF is one of the most popular machine learning algorithms in DSM [81], which is a bagging type ensemble learning method [14]. The advantages of RF over other regression methods are (i) it does not require normally distributed soil data [13], (ii) it can fit complex non-linear relationships between soil data and auxiliary variables, and (iii) the correlation between environmental covariates is not a limiting factor [40]. Then, at second part we used a geostatistical modelling method (ordinary kriging, OK) to spatially extend the derived residuals from RF model [82]. The outcome of the estimation is the sum of the RF model result and the kriged residuals.

2.3.3. Validation of Soil Property Estimations

To assess the performance of the spatial estimation of soil properties a 5-fold cross validation was applied. The following common validation measures were computed: (i) mean error (or bias, ME—Equation (2)) and (ii) root mean square error (RMSE—Equation (3))

$$ME = \frac{1}{n} \sum_{i=1}^n (P_i - O_i) \tag{2}$$

$$RMSE = \sqrt{\frac{1}{n} \sum_{i=1}^n (P_i - O_i)^2} \tag{3}$$

where n is the number of observations; P_i and O_i are the predicted and observed soil property for observation location, respectively.

The methodological steps of data processing are summarized in Figure 2.

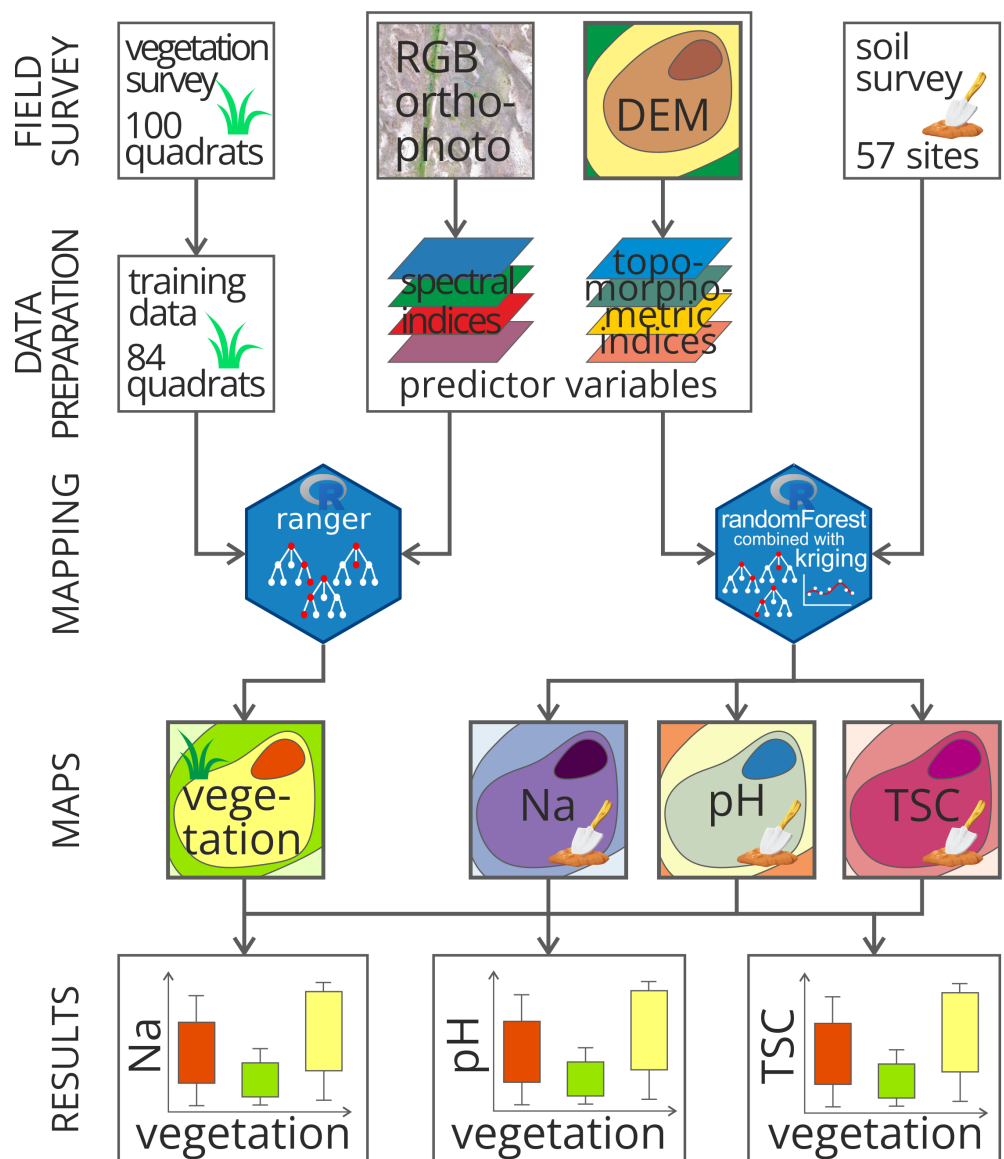


Figure 2. Methodological flowchart of the research work.

3. Results

3.1. Vegetation Map

Figure 3 represents the final vegetation/habitat type map (Table S1). Generally, it resembles the DEM of the area: Achillea steppes (F1b) and closed steppes (H5a) can be found on the highest levels (eastern side and southwestern corner), salt marshes (B6) surrounded by salt meadows (F2) in their foregrounds dominates the lower levels (southern and center part). The intermediate, transitional zones are covered by the annual salt pioneer swards of steppes and lakes (F5) class where the surface is dissected by small canals (on the southern and northern side of the center area). The patches of bare spot can be found in these latter areas.

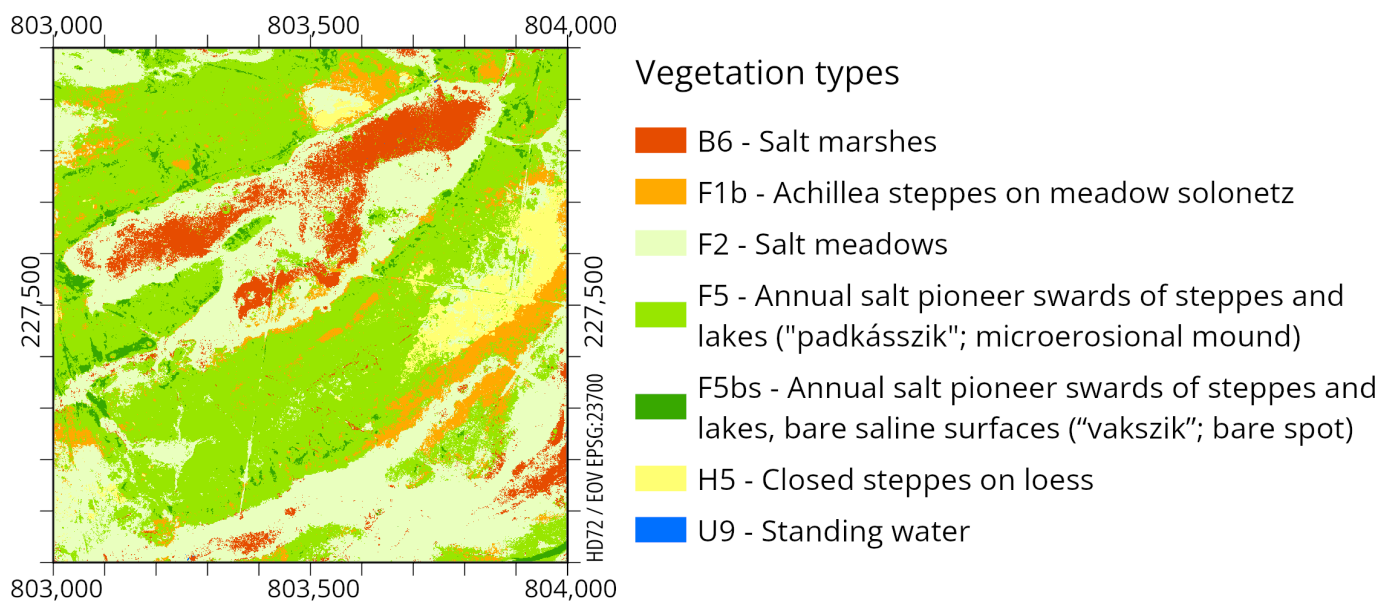


Figure 3. Classified habitat type map.

Analyzing the most important co-variables of the developed classifier model, it indicates the importance of morphometric variables (CNBL, DEM, MRRTE, and MRVBF; Table 2) in the top four position (Figure 4), followed by spectral variables of red, green, and blue bands and BI, VVI, and GLI. In summary, the morphometric variables can be useful to differentiate between habitats located on different altitude levels, RGB bands, and vegetation related spectral indices to separate various plant types and finally brightness index can highlight the bare spot because of their greyish-white surfaces. The bare spots are covered by Solonetz soils, where the Natric horizon is located either immediately on the surface or in close proximity. These spots remain bare due to the aggregate-dispersing effect caused by high sodicity, measured right at the surface. As Natric horizons exhibit the highest salt accumulation within the soil profile, their exposure leads to the highest salinity levels observed within the study site.

Furthermore, the map was tested against the test dataset also, with an average accuracy of 0.988 together with a Kappa value of 0.985. According to the detailed, by class accuracy metrics, the built-up classifier performed a very good classification in each habitat type class with balanced accuracy, precision, and recall values higher than 0.95.

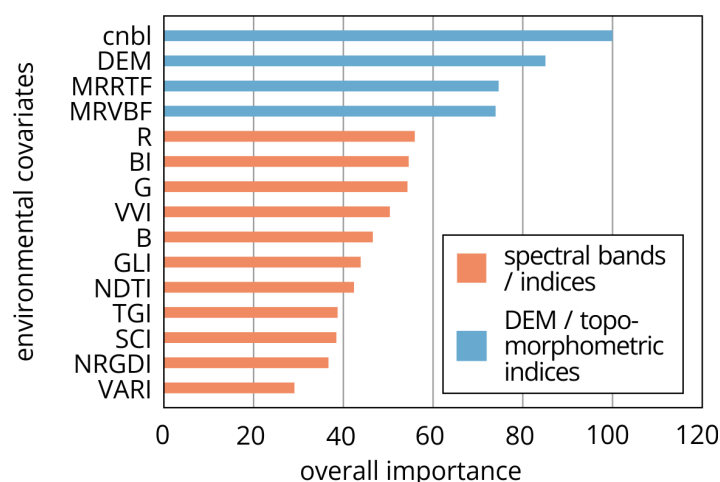


Figure 4. Variable importance of co-variables of the developed classifier model applied in vegetation mapping.

The standing water (U9) class had a perfect classification with balanced accuracy, precision, and recall values of 1.000 thankfully to its completely distinct characteristics and because it was over-represented in the training dataset compared to its spatial coverage on the study site (Table 4). The closed steppes on loess (H5a) had the same values, except balanced accuracy of 0.999. However, the H5a class is located strictly on the higher levels of altitude, making the class again a very distinct one. From the salt-related categories salt marshes (B6) were misclassified only with salt meadows (F2): 2 F2 data points as false positives to B6 salt marshes and 15 B6 test data as false negative to F2 salt meadows. While latter ones are generally located around salt marshes, both type of misclassifications could have happened on their mating edges. Because of the spectral similarity of the vegetation in the middle of spring, F2 points were also classified to F1b Achillea steppes (8) and F5 annual salt pioneer swards of steppes (5) habitat types; however, with 2341 true positive predictions, they still result in a balanced accuracy value of 0.995. Achillea steppes areas (F1b) are cross-misclassified with salt meadows (F2) and annual salt pioneer swards (F5) but the number of both false predictions are twice to the latter category than to F2 class. The reason behind this can be that F1b covered areas are “trapped” between these two habitats. However, despite of adjacent neighborhood with H5a closed steppes habitat in the eastern side of study site, there is no mixed classification with this class probably because of the completely different altitude levels what F1b (mean value: 86.86 m) and H5a (mean value: 87.16 m) habitats are occupied. Regarding the annual salt pioneer swards (F5) to bare spots (F5bs), latter is misclassified with only the F5 class in 36 test points, falsely predicted as F5 class and 11 F5 points falsely classified to F5bs class. The ratio of false predictions shows that F5bs misclassification to F5 category is three times more likely than in the other direction, resulting in the underestimation and underrepresentation of bare spots in the study area. The reason behind this can be that bright color of spots is very distinct compared to other classes (e.g., various kinds of green vegetation and dark water surfaces) but in topomorphometric properties, it is similar to F5 thus they are overlapping with each other in this domain.

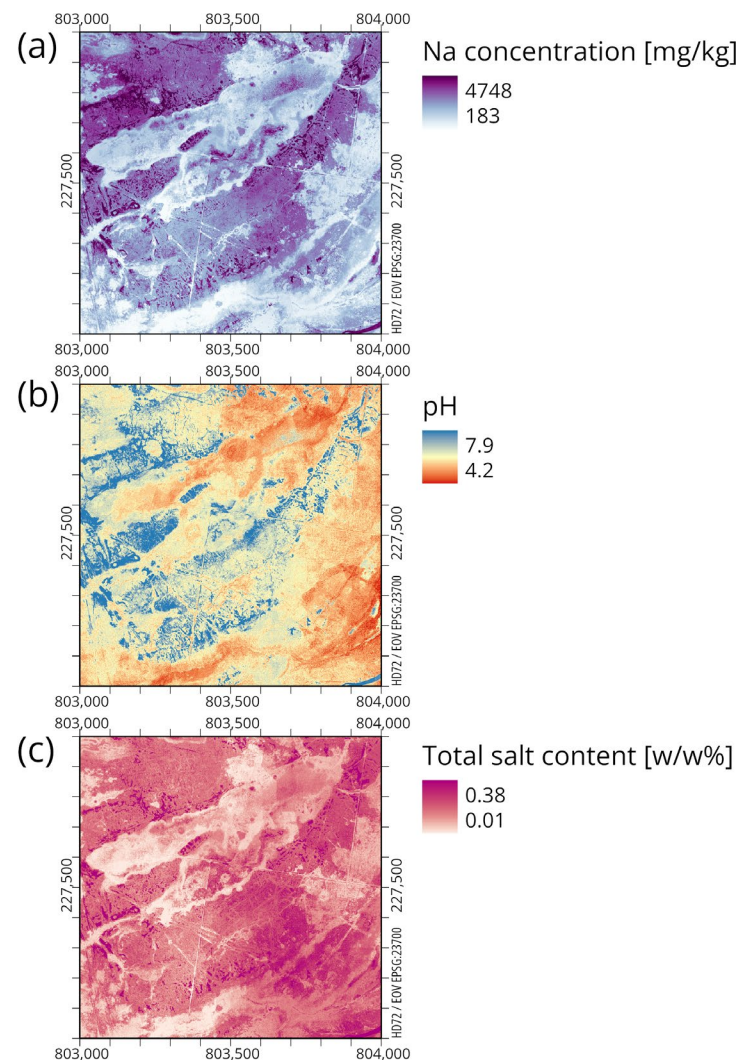
The complete confusion matrix and detailed accuracy metrics of habitat type classes can be found in the Supplementary Materials (Tables S2 and S3).

Table 4. Area ratios of habitat categories in the study area according to the classified vegetation map.

Habitat Code	Area (m ²)	Percent (%)
B6	82,825.25	8.28
F1b	102,861.25	10.29
F2	314,694.75	31.47
F5	439,985.75	44.00
F5bs	24,518.50	2.45
H5a	34,991.75	3.50
U9	122.75	0.01

3.2. Thematic Soil Maps

Figure 5 represents the results of soil property predictions for the study area. Soil properties were estimated independently, but the expected relationship between soil properties is clearly shown in the maps; areas with higher Na concentration also exhibit elevated TSC and increased (even alkaline) pH levels (Table S4).

**Figure 5.** Soil property maps. (a) Na concentration; (b) pH; (c) total salt content.

The findings of variables importance of this study indicate that spectral indices found to be more informative than topomorphometric indices. Among the various spectral indices examined, including SHP, BI, TGI, GLI, VVI, RI, SI, B, CI, and SAT, these indices consistently ranked within the top 15 for every soil property under investigation (Figure 6).

The difference with the important variables of the classification in the previous section can be noted. While ranger is also random forest based algorithm [78], it can sort the covariates by importance summing the individual trees. Our examination showed that morphometric variables can separate the most distinct habitat types (e.g., water, salt marshes, and vegetation related habitats) at first on higher level of trees and on lower levels (on the leaves) vegetation related indices and spectral bands are more important to differentiate between various saline vegetation habitats. However, predicting a continuous numerical value is quite the opposite: in case of the three saline related parameters the fine spatial transitions in values indicated by changing which plant types (highlighted by vegetation indices) received the most importance, supplemented by topographic layers (DEM, CNBL, MRVBF, ASPECT, SPI, SAGAWI, SR, TWI, TRI, SL, and SLOPE) for the sudden changes (mostly found on areas with microerosional mounds).

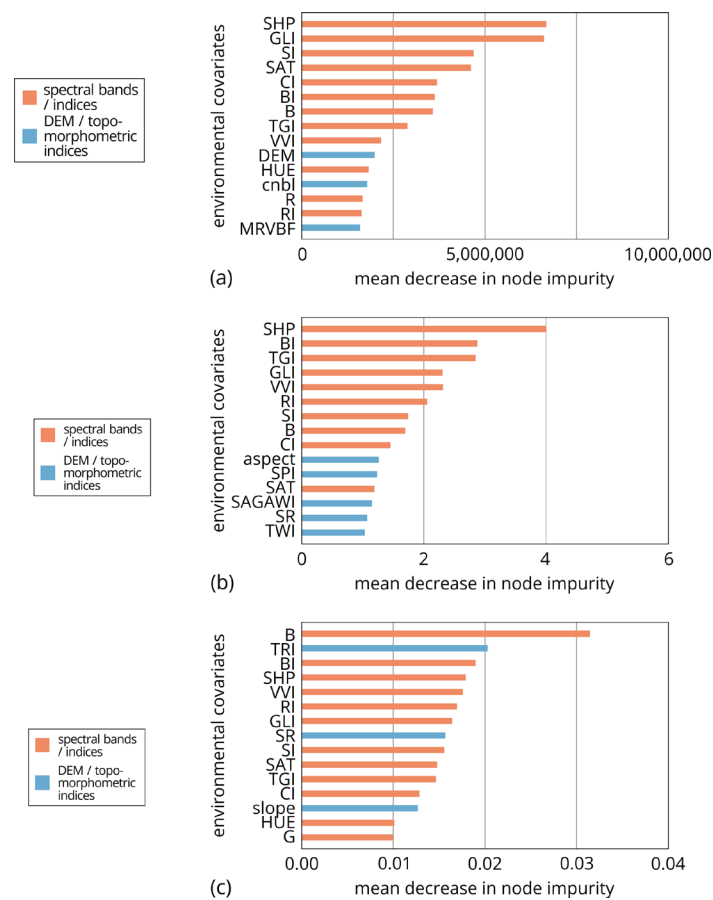


Figure 6. Variable importance. (a) Na; (b) pH; (c) TSC.

Validation results were assessed by a 5-fold cross validation and summarized in Table 5.

Table 5. Validation results of soil property estimations.

Delete Column	Na	pH	TSC
ME	19.10	0.03	−0.00
RMSE	971.45	0.88	0.09

The mean Na concentration is 1959 mg/kg for the whole study area. The northwest part demonstrates a significant concentration of Na, but smaller patches of high Na content observed in the northeastern and southern parts as well. The average pH value for the study area is 5.76. Similar to Na content, more alkaline pH levels are predominantly observed in

the northwest with mosaic-like distribution in the south and northeast. The mean TSC is 0.14 $w/w\%$. In case of TSC, larger areas with higher-than-average TSC values can be found in the southern part, accompanied by smaller spots in the west and the northeast.

Overlapping the three thematic soil maps (Na, pH, and TSC) with the vegetation map, we obtained predicted statistics of soil parameters for each distinct habitat type (Figure 7).

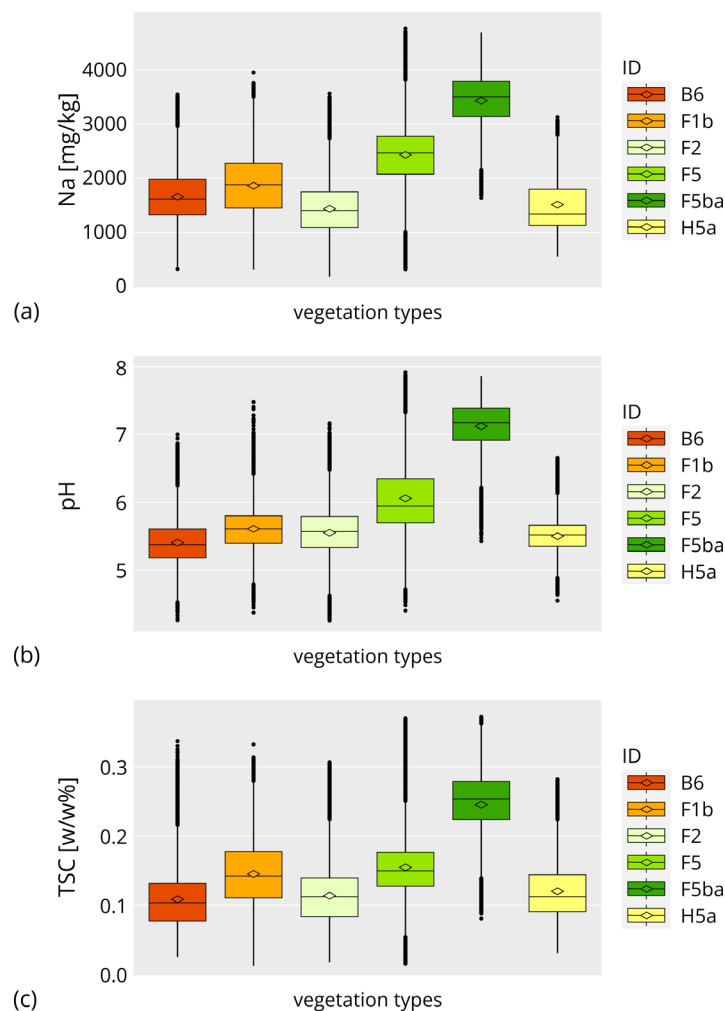


Figure 7. Boxplots of SAS parameters separated according to habitat types. (a) Na; (b) pH; (c) TSC. Legend: codes of Á-NÉR system: B6: salt marshes; F1b: *Achillea* steppes on *Meadow solonetz*; F2: salt meadow; F5: annual salt pioneer swards of steppes and lakes (“*padkásszik*” = microerosional mound); F5bs: annual salt pioneer swards of steppes and lakes, bare spot (“*vakszik*”); H5a: closed steppes on loess.

Salt marshes (B6), covering 8% of the area (Table 4), are intrazonal habitats generally characterized by strongly saline soils (Solonchaks) and vegetation coverage with saline water for a significant period of the growing season [52]. A significant portion of the water that provides moisture to the habitat may originate from the groundwater, which is also the source of the salts causing salinity. In our case, since the water in the area was partly derived from precipitation during the sampling period, the salts—that were previously present in the area in large quantities in the soil—were diluted and leached out. Therefore, the salt content is lower, categorizing it in the moderately saline range (0.075–0.13 $w/w\%$). The relatively high sodium concentration indicates that a significant portion of the salts is sodium-based (1322–1976 mg/kg). These facts are consistent with the observation of [83], stating that compared with other salt lakes and marshes of the world, the alkaline lakes in Hungary are characterized by lower salt content but higher alkalinity. The formation and

persistent existence of the habitat are linked to high groundwater levels and evaporative water management.

Achillea steppe in *Meadow solonetz* (F1b) (Endoprotocalcic Epistagnic Solonetz (Albic, Katoclayic) (Table S5) classified according to [48]) are steppe-like communities, which depend on adequate water supply and moderately saline soil conditions [52,53]. It occupies 10% of the total sampling area (Table 4) and characterized by species that tolerate long summer droughts and heavy textured soils. Since sodium-rich groundwater (Na 1170 mg/kg, SAR 26.5, EC 5.8 dS/m, Table S6) is present at shallow depths (3.3 m) and due to its mid-elevation position within the vegetation zone, this habitat type is the most exposed to salt accumulation in the groundwater fluctuation zone. A total of 1444–2264 mg/kg adsorbed sodium was detected in the soil (TSC: 0.11–0.18 *w/w%*), which tend to accumulate in higher amounts in the deeper layers, resulting in 5.4–5.8 pH in the topsoil. These habitats form a transition between meadows and loess grasslands in terms of water balance, dominated by generalist plant species.

The appearance of salt meadows (F2) (31.5% coverage, Table 5) requires adequate water supply and moderately saline soil. They are tall grasslands that are temporarily covered with water during the initial stages of the growing season (Figure 1c). They develop on wet areas and variously *Saline meadow* or *Solonchak* soils [52,53], in this case it was formed on Endoprotocalcic Protostagnic Solonetz (Albic, Epiloamic, Katoclayic) classified according to [48]. These habitats are widespread on saline soils throughout the Great Hungarian Plain and in many other countries in Europe as well. The soil of salt meadows is often less calcareous, with the upper 5–10 cm layer having higher organic matter content, resulting in 5.3–5.7 pH. While they are typically found on *Solonetz* soils, the characteristics of both *Solonetz* and *Solonchak* soils often coexist, resulting in transitional phenomena. Therefore, compared to other parts of the sampling area, sodium concentration is moderate (1086–1747 mg/kg). Ground water level of the soil of this habitat is 3.6 m depth, having 9.58 SAR value and 1.4 dS/m EC carrying moderate sodification effect (based on [77]). Salt meadows are situated between salt marshes and *Festuca pseudovina*-saline steppes, often alternating with salt pans in a fully developed zonation [52].

The areas of microerosional mound (F5) surrounding the bare spots are the vegetation zone with the largest extent (~44%, Table 3) in the sample area. The highs and lows show a regular repeating pattern of several plant communities that make up a mosaic. The soil chemistry is more variable than in other habitat types, with a pH ranging from 5.69 to 6.34. In terms of salt content, it can be clearly distinguished from bare spots, which contain on average 0.1% more salt (TSC: 0.13–0.18 *w/w%*). The Na content of the soil is 2067–2764 mg/kg, which is lower than that of the bare spot, but higher than that of the soils in other surrounding habitats. Annual salt pioneer swards of steppes and lakes evolved on Endoprotocalcic Solonetz (Albic, Katoclayic, Humic) soil classified according to [48], having a groundwater depth of 4.39 m, and SAR value of groundwater 11, which represents sodic hazard in the deeper soil layers.

Based on the boxplots shown in Figure 7, the bare spot (F5bs) exhibits the highest pH value (6.91–7.39), total salt content (0.22–0.28 *w/w%*), and sodium concentration (3100–3800 mg/kg) inside the study area, followed by the microerosional mound (F5), indicating a correlation between the soils of these interconnected habitats. These findings are consistent with the descriptions by [52,53]. Bare spots on the salt steppe vegetation cover the smallest percentage of the overall sample area (2.45%, Table 3). However, this feature is the most distinctive characteristic of the habitat, typically found in drier sections of the saline slope and saline zone at mid-elevation positions. The presence of bare spots is closely associated with areas with evaporative water management, contributing to their persistence. The habitat type found on bare spots is primarily shaped by the intensive effects of trampling, including herd paths and herding routes. They form small patches with low species diversity, in each and every instance displaying bare soil surfaces, making them reliably estimable using spectral indices [84–86]. Bare spot serves as distinctive elements of the saline vegetation zonation, holding significant landscape importance characterized by

strong patches and mosaic-like patterns. Due to bare spot forming small patches inside the landscape, spatial resolution of our vegetation map was 0.5 m in order to accurately represent this habitat type alongside other, more extensive saline habitats.

The closed steppes on loess (H5a), representing 3.5% of the sampling area (Table 5), occur on loess or other soft bedrock-derived soils [52], in our case, on elevated ridges protruding from the saline steppes. As shown in Figure 8, the highest elevations within the study area are occupied by closed steppes on loess, based on the DEM created for the sampling area. Originally, these habitats are characteristic of areas with higher organic matter content and prone to erosion. Therefore, the sodium content (1128–1793 mg/kg) and salt content (0.09–0.14 *w/w%*) are moderate, while the pH (5.34–5.66) is lower than the average value typical for the area.

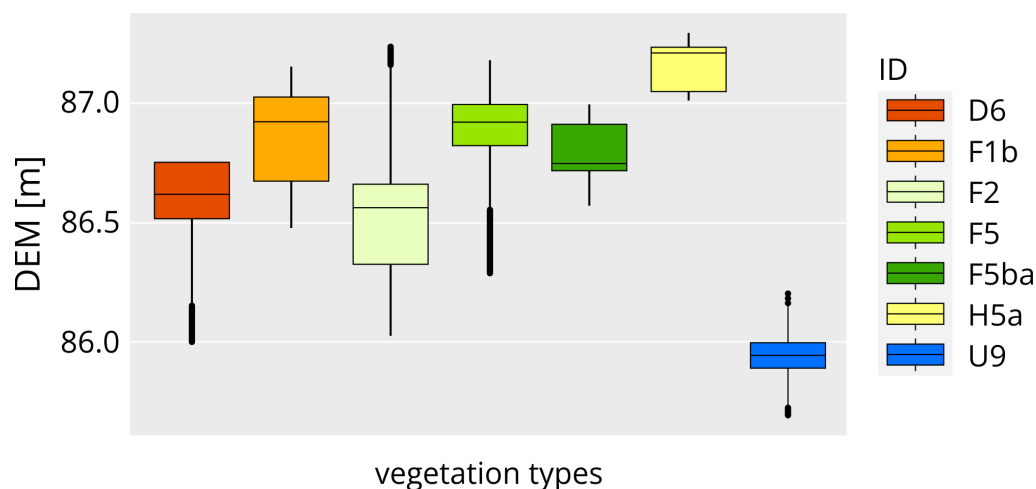


Figure 8. The arrangement of habitats by surface elevation (maBI) based on DEM. Legend: codes of Á-NÉR system: B6: salt marshes; F1b: Achillea steppes on *Meadow solonetz*; F2: salt meadow; F5: annual salt pioneer swards of steppes and lakes (“*padkásszik*” = microerosional mound); F5bs: annual salt pioneer swards of steppes and lakes, bare spot (“*vakszik*”); H5a: closed steppes on loess; U9: standing waters.

We conducted statistical analysis using boxplots to examine the relationship between thematic maps of salt affected soil indicators (pH, Na, and TSC) and habitat map patterns. Through our model-based estimation, we achieved successful indirect estimation of these SAS indicators for each specific habitat type, establishing characteristic thresholds for the soil parameters (Table 6, Figure S1).

Table 6. Summary table of the vegetation map-based SAS indicator estimation of the soils of the different Á-NÉR habitats.

Habitat Types	Á-NÉR Codes	TSC (<i>w/w%</i>)		Na (mg/kg)		pH	
		Threshold					
		Low	High	Low	High	Low	High
Salt marshes	B6	0.08	0.13	1322.74	1976.77	5.18	5.60
Achillea steppes on <i>Meadow solonetz</i>	F1b	0.11	0.18	1444.19	2264.35	5.40	5.80
Salt meadow	F2	0.08	0.14	1085.91	1747.34	5.32	5.79
Annual salt pioneer swards of steppes and lakes (microerosional mound)	F5	0.13	0.18	2067.34	2763.57	5.69	6.34
Annual salt pioneer swards of steppes and lakes (bare spot)	F5bs	0.22	0.28	3126.08	3776.23	6.91	7.39
Closed steppes on loess	H5a	0.09	0.14	1128.18	1793.46	5.35	5.66
Standing waters	U9	0.09	0.15	861.18	1639.39	4.86	5.45

4. Discussion

Several studies have been carried out on remote sensing of salt affected soils and its applicability, e.g., for estimating plant cover [87], for monitoring [88,89], combining with salt movement modelling [90], or testing salinity indices [91]. The applied method, UAV-based multispectral imagery is widespread, but is mostly used to solve problems in precision agriculture [92], e.g., estimate vegetation quality [93], nitrogen content of crops [94,95], or monitoring crop diseases [96]. Our approach involves the creation of a SAS vegetation map using 16 different spectral vegetation indices (VVI, VARI, NDTI, RI, SCI, BI, SI, TGI, GLI, NGRDI, GLAI, HUE, CI, HI, SHP, and SAT) and the calculation of a DEM from RGB orthophoto mosaics as a result of aerial survey using a UAV. Through field observations, we identified distinct habitat types based on the General National Habitat Classification System of Hungary [52], with quadrats representing specific plant species providing crucial data for our predictive model development. By integrating topomorphometric and spectral indices and applying random forest [97] and co-kriging methods [98], we estimated soil properties and generated thematic maps of salt-affected indicators (pH, TSC, and Na), validated using 57 soil samples from the field. Boxplots were generated in order to estimate the pH, TSC and Na concentration range in the soil under different vegetation patterns.

In the Hortobágy microregion, as well as in numerous other European salt steppes [99], the natural process of soil formation exhibits diverse patterns [100]. In certain instances, there is a gradual accumulation of salts, leading to progressive salinization, while in others, leaching and desalinization occur [5,101]. These processes not only manifest in spatial variations but, as described by [102,103], they also display temporal dynamics within specific areas. The alternation of leaching and salt accumulation is influenced by environmental conditions (e.g., hydrological conditions and texture [104] and shapes the characteristics of the developing saline soils [105].) Our research, as indicated by the boxplots at Figure 6, also demonstrates substantial variability and dispersion in soil salinity, sodium content, and pH within specific habitats. For instance, in bare spot (F5bs), there is a prevailing accumulation of salts in the topsoil, resulting in higher salinity and pH, and also sodium content due to Na-salts [106,107]. Conversely, in elevated and more exposed areas, e.g., closed steppes on loess (H5a) (Figure 8), as well as in *Solonetz* soils, the salinity, sodium content, and pH of the topsoil are all lower [108,109]. In these cases, the influence of humus content is also apparent.

The zonation of saline habitats, as determined by the increase in surface elevation, follows the sequence of salt meadow (F2) < salt marshes (B6) < annual salt pioneer swards of steppes and lakes, bare spots (F5bs) < annual salt pioneer swards of steppes and lakes (F5) = *Achillea* steppes on *Meadow solonetz* (F1b) < closed steppes on loess (H5a) (see Figure 8). This order of zonation aligns with the findings of [110,111]. The highest salt content, sodium content, and pH, considering the zonation of the area, are observed in the soils of vegetation belts located in the intermediate positions [112,113].

The novelty of our work is to employ a cost-effective and straightforward approach utilizing multispectral RGB imaging to produce a highly accurate (98.8%) vegetation map of the salt steppe.

Habitat types in the Hungarian General National Habitat Classification System (Á-NÉR [52]) are associated with specific soil types. Our research introduces a novel aspect by offering threshold values for salinity, sodicity, and alkalinity indicators (Na, TSC, and pH) corresponding to the saline habitat types in Á-NÉR. To estimate these values, we utilized a model combining the random forest and kriging (RFK) methods.

The study area we investigated is situated within Europe's largest continuous natural semi-arid steppe, which represents extensive Eurasian steppes with similar characteristics. Our modelling method can form the basis for the proximal, non-invasive surveying of protected saline areas and the model estimation of salinity indicators.

5. Conclusions

- The analysis of the classifier model's ("ranger" machine learning) most important co-variables in case of preparing vegetation map, highlights the significance of morphometric variables (CNBL, DEM, MRRTF, and MRVBF) in the top four positions, followed by spectral variables (red, green, blue bands, BI, VVI, and GLI). Morphometric variables differentiate habitats based on altitude levels, while RGB bands and vegetation-related spectral indices separate different plant types. The BI is particularly useful in identifying bare spots with greyish-white surfaces. The applied geostatistical model demonstrated high accuracy (0.9889) and a Kappa value of 0.9857 when tested against the dataset. The classification performance for each habitat type was excellent, with balanced accuracy, precision, and recall values exceeding 0.95.
- Correlation analysis of thematic maps of SAS indicators (pH, Na, and TSC) and habitat map patterns was carried out applying boxplots. Our model-based estimation was successful to indirectly estimate these SAS indicators for every distinct habitat type, defining characteristic thresholds for the soil parameters.
- For UAV-based RGB orthophotos, it was found that spectral indices (SHP, BI, TGI, GLI, VVI, RI, SI, B, CI, and SAT) provided more comprehensive information compared to topomorphometric indices when considering the importance of the variables in estimating all SAS parameters.

Supplementary Materials: The following supporting information can be downloaded at: <https://www.mdpi.com/article/10.3390/land12081516/s1>, Table S1: Summary table of the quadrat vegetation survey, forming the base data for the vegetation map. Table S2: Confusion matrix of test dataset with reference (columns) and predicted (rows) comparison. Table S3: Detailed accuracy metrics by class. Table S4: Laboratory measured soil parameters applied in thematic mapping. Table S5: Site Soil Investigation Reports of the 3 soil Profiles. Table S6: Groundwater chemistry data. Figure S1: 3D scatterplot of the represented habitat types in the light of the three mapped soil salinity parameters.

Author Contributions: L.P.: conceptualization, validation, formal analysis, resources, writing—review and editing, supervision, and funding acquisition. K.T.: conceptualization, visualization, software, formal analysis, methodology, and writing—review and editing. J.M.: field measurement and observation, methodology, software, formal analysis, validation, data curation, resources, writing—original draft preparation, and writing—review and editing. G.S.: software, methodology, validation, formal analysis, writing—original draft preparation, writing—review and editing, and visualization. M.Á.: field measurement and observation, methodology, validation, data curation, and visualization. T.T.: conceptualization, validation, formal analysis, field observation and mapping, investigation, supervision, and funding acquisition. G.B.: investigation, methodology, field measurement and observation, and validation. P.L.: field measurement and observation and methodology. Z.A.K.: data curation and investigation. S.K.: field measurement and observation and methodology. K.B.: methodology, validation, writing—original draft preparation, writing—review and editing, and project administration. All authors have read and agreed to the published version of the manuscript.

Funding: This research was funded by the National Research, Development and Innovation Office (NKFIH), grant number K-124290.

Data Availability Statement: The data presented in this study are available in Supplementary Materials.

Acknowledgments: We would like to thank the Hortobágy National Park for allowing us to carry out the investigation on its Natura 2000 site. Special thanks to Tibor József Novák for his help in the field works. The work of Gábor Szatmári was supported by the János Bolyai Research Scholarship of the Hungarian Academy of Sciences.

Conflicts of Interest: The authors declare no conflict of interest.

References

1. Montoroi, J.-P. Soil Salinization and Management of Salty Soils. In *Soils as a Key Component of the Critical Zone 5: Degradation and Rehabilitation. Geosciences Series. Soils Set*; Valenton, C., Ed.; ISTE, Wiley: London, UK, 2018; pp. 97–126.
2. Zhao, M.; Wang, C.; He, Y.; He, T. Soil Characteristics and Response Thresholds of Salt Meadow on Lake Beaches of the Ordos Platform. *Front. Environ. Sci.* **2022**, *10*, 1050757. [[CrossRef](#)]
3. Lubińska-Mielińska, S.; Kački, Z.; Kamiński, D.; Pétilion, J.; Evers, C.; Piernik, A. Vegetation of Temperate Inland Salt-Marshes Reflects Local Environmental Conditions. *Sci. Total Environ.* **2023**, *856*, 159015. [[CrossRef](#)]
4. IMEUH. *Interpretation Manual of European Union Habitats*; European Commission: Brussels, Belgium, 2007.
5. Ladányi, Z.; Balog, K.; Tóth, T.; Barna, G. Longer-Term Monitoring of a Degrading Sodic Lake: Landscape Level Impacts of Hydrological Regime Changes and Restoration Interventions (SE Hungary). *Arid. Land Res. Manag.* **2023**, *37*, 389–407. [[CrossRef](#)]
6. Eswar, D.; Karuppusamy, R.; Chellamuthu, S. Drivers of Soil Salinity and Their Correlation with Climate Change. *Curr. Opin. Environ. Sustain.* **2021**, *50*, 310–318. [[CrossRef](#)]
7. Schofield, R.V.; Kirkby, M.J. Application of Salinization Indicators and Initial Development of Potential Global Soil Salinization Scenario under Climatic Change. *Glob. Biogeochem. Cycles* **2003**, *17*, 4–1–4–13. [[CrossRef](#)]
8. McBratney, A.B.; Mendonça Santos, M.L.; Minasny, B. On Digital Soil Mapping. *Geoderma* **2003**, *117*, 3–52. [[CrossRef](#)]
9. Minasny, B.; McBratney, A.B. Digital Soil Mapping: A Brief History and Some Lessons. *Geoderma* **2016**, *264*, 301–311. [[CrossRef](#)]
10. Szatmári, G.; Bakacsi, Z.; Laborczy, A.; Petrik, O.; Pataki, R.; Tóth, T.; Pásztor, L. Elaborating Hungarian Segment of the Global Map of Salt-Affected Soils (GSSmap): National Contribution to an International Initiative. *Remote Sens.* **2020**, *12*, 4073. [[CrossRef](#)]
11. Gorji, T.; Tanik, A.; Sertel, E. Soil Salinity Prediction, Monitoring and Mapping Using Modern Technologies. *Procedia Earth Planet. Sci.* **2015**, *15*, 507–512. [[CrossRef](#)]
12. Suleymanov, A.; Gabbasova, I.; Komissarov, M.; Suleymanov, R.; Garipov, T.; Tuktarova, I.; Belan, L. Random Forest Modeling of Soil Properties in Saline Semi-Arid Areas. *Agriculture* **2023**, *13*, 976. [[CrossRef](#)]
13. Keskin, H.; Grunwald, S. Regression Kriging as a Workhorse in the Digital Soil Mapper’s Toolbox. *Geoderma* **2018**, *326*, 22–41. [[CrossRef](#)]
14. Szabó, B.; Szatmári, G.; Takács, K.; Laborczy, A.; Makó, A.; Rajkai, K.; Pásztor, L. Mapping Soil Hydraulic Properties Using Random-Forest-Based Pedotransfer Functions and Geostatistics. *Hydrol. Earth Syst. Sci.* **2019**, *23*, 2615–2635. [[CrossRef](#)]
15. Nabiollahi, K.; Taghizadeh-Mehrjardi, R.; Shahabi, A.; Heung, B.; Amirian-Chakan, A.; Davari, M.; Scholten, T. Assessing Agricultural Salt-Affected Land Using Digital Soil Mapping and Hybridized Random Forests. *Geoderma* **2021**, *385*, 114858. [[CrossRef](#)]
16. Heuvelink, G.B.M.; Webster, R. Spatial Statistics and Soil Mapping: A Blossoming Partnership under Pressure. *Spat. Stat.* **2022**, *50*, 100639. [[CrossRef](#)]
17. Metternicht, G.I.; Zinck, J.A. Remote Sensing of Soil Salinity: Potentials and Constraints. *Remote Sens. Environ.* **2003**, *85*, 1–20. [[CrossRef](#)]
18. Mulder, V.L.; de Bruin, S.; Schaepman, M.E.; Mayr, T.R. The Use of Remote Sensing in Soil and Terrain Mapping—A Review. *Geoderma* **2011**, *162*, 1–19. [[CrossRef](#)]
19. Sahbeni, G.; Ngabire, M.; Musyimi, P.K.; Székely, B. Challenges and Opportunities in Remote Sensing for Soil Salinization Mapping and Monitoring: A Review. *Remote Sens.* **2023**, *15*, 2540. [[CrossRef](#)]
20. Ivushkin, K.; Bartholomeus, H.; Bregt, A.K.; Pulatov, A.; Franceschini, M.H.D.; Kramer, H.; van Loo, E.N.; Jaramillo Roman, V.; Finkers, R. UAV Based Soil Salinity Assessment of Cropland. *Geoderma* **2019**, *338*, 502–512. [[CrossRef](#)]
21. Richer-de-Forges, A.C.; Chen, Q.; Baghdadi, N.; Chen, S.; Gomez, C.; Jacquemoud, S.; Martelet, G.; Mulder, V.L.; Urbina-Salazar, D.; Vaudour, E.; et al. Remote Sensing Data for Digital Soil Mapping in French Research—A Review. *Remote Sens.* **2023**, *15*, 3070. [[CrossRef](#)]
22. Dronova, I.; Kislik, C.; Dinh, Z.; Kelly, M. A Review of Unoccupied Aerial Vehicle Use in Wetland Applications: Emerging Opportunities in Approach, Technology, and Data. *Drones* **2021**, *5*, 45. [[CrossRef](#)]
23. Lyu, X.; Li, X.; Dang, D.; Dou, H.; Wang, K.; Lou, A. Unmanned Aerial Vehicle (UAV) Remote Sensing in Grassland Ecosystem Monitoring: A Systematic Review. *Remote Sens.* **2022**, *14*, 1096. [[CrossRef](#)]
24. Wang, Y.; Lu, Z.; Sheng, Y.; Zhou, Y. Remote Sensing Applications in Monitoring of Protected Areas. *Remote Sens.* **2020**, *12*, 1370. [[CrossRef](#)]
25. Zhang, J.; Okin, G.S.; Zhou, B.; Karl, J.W. UAV-Derived Imagery for Vegetation Structure Estimation in Rangelands: Validation and Application. *Ecosphere* **2021**, *12*, e03830. [[CrossRef](#)]
26. Zhang, H.; Feng, Y.; Guan, W.; Cao, X.; Li, Z.; Ding, J. Using Unmanned Aerial Vehicles to Quantify Spatial Patterns of Dominant Vegetation along an Elevation Gradient in the Typical Gobi Region in Xinjiang, Northwest China. *Glob. Ecol. Conserv.* **2021**, *27*, e01571. [[CrossRef](#)]
27. Lehmann, J.R.K.; Prinz, T.; Ziller, S.R.; Thiele, J.; Heringer, G.; Meira-Neto, J.A.A.; Buttschardt, T.K. Open-Source Processing and Analysis of Aerial Imagery Acquired with a Low-Cost Unmanned Aerial System to Support Invasive Plant Management. *Front. Environ. Sci.* **2017**, *5*, 44. [[CrossRef](#)]
28. Mustaffa, A.A.; Mukhtar, A.N.; Rasib, A.W.; Suhandri, H.F.; Bukari, S.M. Mapping of Peat Soil Physical Properties by Using Drone- Based Multispectral Vegetation Imagery. *IOP Conf. Ser. Earth Environ. Sci.* **2020**, *498*, 012021. [[CrossRef](#)]

29. Oh, S.; Chang, A.; Yang, Y.E.; Kim, H.S.; Lim, K.J.; Jung, J. Recent Advances in UAS Based Soil Erosion Mapping. *Mod. Concepts Dev. Agron.* **2020**, *7*. [[CrossRef](#)]
30. Takata, Y.; Yamada, H.; Kanuma, N.; Ise, Y.; Kanda, T. Digital Soil Mapping Using Drone Images and Machine Learning at the Sloping Vegetable Fields in Cool Highland in the Northern Kanto Region, Japan. *Soil Sci. Plant Nutr.* **2023**, *69*, 221–230. [[CrossRef](#)]
31. Bertalan, L.; Holb, I.; Pataki, A.; Szabó, G.; Kupásné Szalóki, A.; Szabó, S. UAV-Based Multispectral and Thermal Cameras to Predict Soil Water Content—A Machine Learning Approach. *Comput. Electron. Agric.* **2022**, *200*, 107262. [[CrossRef](#)]
32. Wei, G.; Li, Y.; Zhang, Z.; Chen, Y.; Chen, J.; Yao, Z.; Lao, C.; Chen, H. Estimation of Soil Salt Content by Combining UAV-Borne Multispectral Sensor and Machine Learning Algorithms. *PeerJ* **2020**, *2020*, e9087. [[CrossRef](#)] [[PubMed](#)]
33. Ma, Y.; Zhu, W.; Zhang, Z.; Chen, H.; Zhao, G.; Liu, P. Fusion Level of Satellite and UAV Image Data for Soil Salinity Inversion in the Coastal Area of the Yellow River Delta. *Int. J. Remote Sens.* **2022**, *43*, 7039–7063. [[CrossRef](#)]
34. Kahaer, Y.; Tashpolat, N. Estimating Salt Concentrations Based on Optimized Spectral Indices in Soils with Regional Heterogeneity. *J. Spectrosc.* **2019**, *15*, 2402749. [[CrossRef](#)]
35. Silver, M.; Tiwari, A.; Karnieli, A. Identifying Vegetation in Arid Regions Using Object-Based Image Analysis with RGB-Only Aerial Imagery. *Remote Sens.* **2019**, *11*, 2308. [[CrossRef](#)]
36. Last, W.M.; Ginn, F.M. Saline Systems of the Great Plains of Western Canada: An Overview of the Limnogeology and Paleolimnology. *Saline Syst.* **2005**, *1*, 10. [[CrossRef](#)] [[PubMed](#)]
37. Dítě, D.; Šuvada, R.; Tóth, T.; Dítě, Z. Inventory of the Halophytes in Inland Central Europe. *Preslia* **2023**, *95*, 215–240. [[CrossRef](#)]
38. Deák, B.; Valkó, O.; Alexander, C.; Mücke, W.; Kania, A.; Tamás, J.; Heilmeyer, H. Fine-Scale Vertical Position as an Indicator of Vegetation in Alkali Grasslands—Case Study Based on Remotely Sensed Data. *Flora-Morphol. Distrib. Funct. Ecol. Plants* **2014**, *209*, 693–697. [[CrossRef](#)]
39. Themistocleous, K. DEM Modeling Using RGB-Based Vegetation Indices from UAV Images. In Proceedings of the Seventh International Conference on Remote Sensing and Geoinformation of the Environment (RSCy2019), Paphos, Cyprus, 18–21 March 2019; Themistocleous, K., Papadavid, G., Michaelides, S., Ambrosia, V., Hadjimitsis, D., Eds.; SPIE: Bellingham, WA, USA, 2019; Volume 11174, pp. 499–506.
40. Szatmári, G.; Pásztor, L. Comparison of Various Uncertainty Modelling Approaches Based on Geostatistics and Machine Learning Algorithms. *Geoderma* **2019**, *337*, 1329–1340. [[CrossRef](#)]
41. Wang, L.; Wu, W.; Liu, H. Bin Digital Mapping of Topsoil PH by Random Forest with Residual Kriging (RFRK) in a Hilly Region. *Soil Res.* **2019**, *57*, 387–396. [[CrossRef](#)]
42. Hengl, T.; Nussbaum, M.; Wright, M.N.; Heuvelink, G.B.M.; Gräler, B. Random Forest as a Generic Framework for Predictive Modeling of Spatial and Spatio-Temporal Variables. *PeerJ* **2018**, *2018*, e5518. [[CrossRef](#)]
43. Dövényi, Z. (Ed.) *Magyarország Kistájainak Katasztere [Inventory of Microregions in Hungary]*; MTA Földrajztudományi Intézet: Budapest, Hungary, 2010.
44. Novák, T.J.; Tóth, C.A. Development of Erosional Microforms and Soils on Semi-Natural and Anthropogenic Influenced Solonchic Grasslands. *Geomorphology* **2016**, *254*, 121–129. [[CrossRef](#)]
45. Tóth, C.; Novák, T.; Rakonczai, J. Hortobágy Puszta: Microtopography of Alkali Flats. In *Landscapes and Landforms of Hungary*; Lóczy, D., Ed.; Springer International Publishing: Cham, Switzerland, 2015; pp. 237–246. ISBN 978-3-319-08997-3.
46. Tóth, T.; Szendrei, G. A Sókivirágzások Elterjedésének És Képződésének Összefüggése a Környezeti, Ezen Belül Talajtani Tényezőkkel [Relationship between Salt Efflorescences and Environmental Conditions with Special Emphasis on Edaphological Conditions]. *Topogr. Mineral. Hung.* **2006**, *IX*, 79–90.
47. Tóth, T.; Kuti, L. Összefüggés a Talaj Sótartalma És Egyes Földtani Tényezők Között a Hortobágyi “Nyírölapos” Mintaterületen. I. Általános Földtani Jellemzés, a Felszín Alatti Rétegek Kalcittartalma És PH Értéke [Geological Factors Affecting the Salinization of the Nyírölapos Sample Area (Hortobágy, Hungary). I. General Geological Characterization, Calcite Concentration and PH Values of Subsurface Layers]. *Agrokémia Talajt.* **1999**, *48*, 431–446.
48. IUSS Working Group WRB. *World Reference Base for Soil Resources 2014, Update 2015. World Soil Resources Reports 106*; FAO: Rome, Italy, 2015.
49. Michéli, E.; Fuchs, M.; Hegymegi, P.; Stefanovits, P. Classification of the Major Soils of Hungary and Their Correlation with the World Reference Base for Soil Resources (WRB). *Agrokémia Talajt.* **2006**, *55*, 19–28. [[CrossRef](#)]
50. Gallai, B.; Árvai, M.; Mészáros, J.; Barna, G.; Pásztor, L.; Szatmári, G.; Ulicsni, V.; Tóth, B.; Novák, T.; Tóth, T. A Talaj És Növényzet Összefüggése a Hortobágyi Ágota-Pusztán [The Relationship between Soil and Vegetation Ágota-Puszta, Hortobágy]. In Proceedings of the Talajtani Vándorgyűlés, Sárovar, Hungary, 25 September 2020.
51. Tóth, T.; Rajkai, K. Soil and Plant Correlations in a Solonchic Grassland. *Soil Sci.* **1994**, *157*, 253–262. [[CrossRef](#)]
52. Bölöni, J.; Molnár, Z.; Kun, A. (Eds.) *Magyarország Élőhelyei. A Hazai Vegetációtípusok Leírása És Határozója. ÁNÉR 2011 [Habitats of Hungary]*; MTA Ökológiai és Botanikai Kutatóintézete: Vácrátót, Hungary, 2011.
53. Molnár, Z.; Bíró, M.; Bölöni, J.; Horváth, F. Distribution of the (Semi-)Natural Habitats in Hungary I. Marshes and Grasslands. *Acta Bot. Hung.* **2009**, *50*, 59–105. [[CrossRef](#)]
54. Reudenbach, C.; Meyer, H. UavRst R package: Unmanned Aerial Vehicle Remote Sensing Tools 2022. Available online: <https://gisma.github.io/uavRst/> (accessed on 28 June 2023).
55. Conrad, O.; Bechtel, B.; Bock, M.; Dietrich, H.; Fischer, E.; Gerlitz, L.; Wehberg, J.; Wichmann, V.; Böhner, J. System for Automated Geoscientific Analyses (SAGA) v. 2.1.4. *Geosci. Model Dev.* **2015**, *8*, 1991–2007. [[CrossRef](#)]

56. Mohammadi, H.; Samadzadegan, F. An Object Based Framework for Building Change Analysis Using 2D and 3D Information of High Resolution Satellite Images. *Adv. Space Res.* **2020**, *66*, 1386–1404. [[CrossRef](#)]
57. Gitelson, A.A.; Kaufman, Y.J.; Stark, R.; Rundquist, D. Novel Algorithms for Remote Estimation of Vegetation Fraction. *Remote Sens. Environ.* **2002**, *80*, 76–87. [[CrossRef](#)]
58. Lacaux, J.P.; Tourre, Y.M.; Vignolles, C.; Ndione, J.A.; Lafaye, M. Classification of Ponds from High-Spatial Resolution Remote Sensing: Application to Rift Valley Fever Epidemics in Senegal. *Remote Sens. Environ.* **2007**, *106*, 66–74. [[CrossRef](#)]
59. Madeira, J.; Bedidi, A.; Cervelle, B.; Pouget, M.; Flay, N. Visible Spectrometric Indices of Hematite (Hm) and Goethite (Gt) Content in Lateritic Soils: The Application of a Thematic Mapper (TM) Image for Soil-Mapping in Brasilia, Brazil. *Int. J. Remote Sens.* **1997**, *18*, 2835–2852. [[CrossRef](#)]
60. Novák, J.; Lukas, V.; Kren, J. Estimation of Soil Properties Based on Soil Colour Index. *Agric. Conspec. Sci.* **2018**, *83*, 71–76.
61. Mathieu, R.; Pouget, M.; Cervelle, B.; Escadafal, R. Relationships between Satellite-Based Radiometric Indices Simulated Using Laboratory Reflectance Data and Typic Soil Color of an Arid Environment. *Remote Sens. Environ.* **1998**, *66*, 17–28. [[CrossRef](#)]
62. Raymond Hunt, E.; Daughtry, C.S.T.; Eitel, J.U.H.; Long, D.S. Remote Sensing Leaf Chlorophyll Content Using a Visible Band Index. *Agron. J.* **2011**, *103*, 1090–1099. [[CrossRef](#)]
63. Louhaichi, M.; Borman, M.M.; Johnson, D.E. Spatially Located Platform and Aerial Photography for Documentation of Grazing Impacts on Wheat. *Geocarto Int.* **2001**, *16*, 65–70. [[CrossRef](#)]
64. Tucker, C.J. Red and Photographic Infrared Linear Combinations for Monitoring Vegetation. *Remote Sens. Environ.* **1979**, *8*, 127–150. [[CrossRef](#)]
65. Escadafal, R.; Belghit, A.; Ben-Moussa, A. Indices Spectraux Pour La Télédétection de La Dégradation Des Milieux Naturels En Tunisie Aride. In Proceedings of the Actes du 6eme Symposium International sur les Mesures Physiques et Signatures en Télédétection, Val d'Isère, France, 17–21 January 1994; pp. 253–259.
66. Olaya, V. A Gentle Introduction to SAGA GIS. Available online: <http://sourceforge.net/saga-gis/> (accessed on 28 June 2023).
67. Wilson, J.; Gallant, J. Primary Topographic Attributes. In *Terrain Analysis: Principles and Applications*; Wilson, J., Gallant, J., Eds.; John Wiley & Sons, Inc.: Hoboken, NJ, USA, 2000; p. 520.
68. Riley, S.; DeGloria, S.; Elliot, R. A Terrain Ruggedness Index That Quantifies Topographic Heterogeneity. *Int. J. Sci.* **1999**, *5*, 23–27.
69. Iwahashi, J.; Pike, R.J. Automated Classifications of Topography from DEMs by an Unsupervised Nested-Means Algorithm and a Three-Part Geometric Signature. *Geomorphology* **2007**, *86*, 409–440. [[CrossRef](#)]
70. Olaya, V. Chapter 6 Basic Land-Surface Parameters. *Dev. Soil Sci.* **2009**, *33*, 141–169. [[CrossRef](#)]
71. Böhner, J.; Selige, T. Spatial Prediction of Soil Attributes Using Terrain Analysis and Climate Regionalisation. In *SAGA—Analysis and Modelling Applications. Göttinger Geographische Abhandlungen 115*; Boehner, J., McCloy, K., Strobl, J., Eds.; Geographischen Instituts der Universität Göttingen: Göttingen, Germany, 2006; pp. 13–28.
72. Böhner, J.; AntoniĆ, O. Chapter 8 Land-Surface Parameters Specific to Topo-Climatology. *Dev. Soil Sci.* **2009**, *33*, 195–226. [[CrossRef](#)]
73. Moore, I.D.; Grayson, R.B.; Ladson, A.R. Digital Terrain Modelling: A Review of Hydrological, Geomorphological, and Biological Applications. *Hydrol. Process.* **1991**, *5*, 3–30. [[CrossRef](#)]
74. Friedrich, K. Multivariate Distance Methods for Geomorphographic Relief Classification. In *Land Information Systems—Developments for Planning the Sustainable Use of Land Resources. European Soil Bureau—Research Report 4, EUR 17729 EN*; Heinecke, H., Eckelmann, W., Thomasson, A., Jones, J., Montanarella, L., Buckley, B., Eds.; Office for Official Publications of the European Communities: Ispra, Italy, 1998; pp. 259–266.
75. Gallant, J.C.; Dowling, T.I. A Multiresolution Index of Valley Bottom Flatness for Mapping Depositional Areas. *Water Resour. Res.* **2003**, *39*, 1347. [[CrossRef](#)]
76. Beven, K.J.; Kirkby, M.J. A Physically Based, Variable Contributing Area Model of Basin Hydrology. *Hydrol. Sci. Bull.* **1979**, *24*, 43–69. [[CrossRef](#)]
77. Ayers, R.S.; Westcot, D.W. *Water Quality for Agriculture. FAO Irrigation and Drainage Paper 29 Rev. 1*; FAO: Rome, Italy, 1985.
78. Wright, M.N.; Ziegler, A. Ranger: A Fast Implementation of Random Forests for High Dimensional Data in C++ and R. *J. Stat. Softw.* **2017**, *77*, 1–17. [[CrossRef](#)]
79. Kuhn, M. Building Predictive Models in R Using the Caret Package. *J. Stat. Softw.* **2008**, *28*, 1–26. [[CrossRef](#)]
80. Breiman, L. Random Forests. *Mach. Learn.* **2001**, *45*, 5–32. [[CrossRef](#)]
81. Hengl, T.; MacMillan, R.A. *Predictive Soil Mapping with R*; OpenGeoHub Foundation: Wageningen, The Netherlands, 2019.
82. Hengl, T. *A Practical Guide to Geostatistical Mapping of Environmental Variables. EUR 22904 EN*; Office for Official Publications of the European Communities: Luxembourg, 2007; ISBN 978-92-79-06904-8.
83. Šefferová Stanová, V.; Janák, M.; Ripka, J. *Management of Natura 2000 Habitats. 1530 *Pannonic Salt Steppes and Salt Marshes*; Technical Report; European Commission: Brussels, Belgium, 2008; Available online: https://ec.europa.eu/environment/nature/natura2000/management/habitats/pdf/1530_Pannonic_salt_steppes.pdf (accessed on 28 June 2023).
84. Elnaggar, A.A.; Noller, J.S. Application of Remote-Sensing Data and Decision-Tree Analysis to Mapping Salt-Affected Soils over Large Areas. *Remote Sens.* **2009**, *2*, 151–165. [[CrossRef](#)]
85. Zhang, Z.; Niu, B.; Li, X.; Kang, X.; Hu, Z. Estimation and Dynamic Analysis of Soil Salinity Based on UAV and Sentinel-2A Multispectral Imagery in the Coastal Area, China. *Land* **2022**, *11*, 2307. [[CrossRef](#)]

86. Zhao, W.; Zhou, C.; Zhou, C.; Ma, H.; Wang, Z. Soil Salinity Inversion Model of Oasis in Arid Area Based on UAV Multispectral Remote Sensing. *Remote Sens.* **2022**, *14*, 1804. [[CrossRef](#)]
87. Tóth, T.; Csillag, F.; Biehl, L.L.; Michéli, E. Characterization of Semivegetated Salt-Affected Soils by Means of Field Remote Sensing. *Remote Sens. Environ.* **1991**, *37*, 167–180. [[CrossRef](#)]
88. Mougenot, B.; Pouget, M. Remote Sensing of Salt Affected Soils. *Remote Sens. Rev.* **1993**, *7*, 241–259. [[CrossRef](#)]
89. Tóth, T.; Kertész, M.; Pásztor, L. New Approaches in Salinity/Sodicity Mapping in Hungary. *Agrokémia Talajt.* **1998**, *47*, 76–86.
90. Farifteh, J.; Farshad, A.; George, R.J. Assessing Salt-Affected Soils Using Remote Sensing, Solute Modelling, and Geophysics. *Geoderma* **2006**, *130*, 191–206. [[CrossRef](#)]
91. Jamali, A.A.; Montazeri Naeni, M.A.; Zarei, G. Assessing the Expansion of Saline Lands through Vegetation and Wetland Loss Using Remote Sensing and GIS. *Remote Sens. Appl.* **2020**, *20*, 100428. [[CrossRef](#)]
92. Benos, L.; Tagarakis, A.C.; Dolias, G.; Berruto, R.; Kateris, D.; Bochtis, D. Machine Learning in Agriculture: A Comprehensive Updated Review. *Sensors* **2021**, *21*, 3758. [[CrossRef](#)]
93. García-Fernández, M.; Sanz-Ablanedo, E.; Rodríguez-Pérez, J.R. High-Resolution Drone-Acquired RGB Imagery to Estimate Spatial Grape Quality Variability. *Agronomy* **2021**, *11*, 655. [[CrossRef](#)]
94. Fu, Z.; Yu, S.; Zhang, J.; Xi, H.; Gao, Y.; Lu, R.; Zheng, H.; Zhu, Y.; Cao, W.; Liu, X. Combining UAV Multispectral Imagery and Ecological Factors to Estimate Leaf Nitrogen and Grain Protein Content of Wheat. *Eur. J. Agron.* **2022**, *132*, 126405. [[CrossRef](#)]
95. Li, Z.; Zhou, X.; Cheng, Q.; Fei, S.; Chen, Z. A Machine-Learning Model Based on the Fusion of Spectral and Textural Features from UAV Multi-Sensors to Analyse the Total Nitrogen Content in Winter Wheat. *Remote Sens.* **2023**, *15*, 2152. [[CrossRef](#)]
96. Yamamoto, S.; Nomoto, S.; Hashimoto, N.; Maki, M.; Hongo, C.; Shiraiwa, T.; Homma, K. Monitoring Spatial and Time-Series Variations in Red Crown Rot Damage of Soybean in Farmer Fields Based on UAV Remote Sensing. *Plant Prod. Sci.* **2023**, *26*, 36–47. [[CrossRef](#)]
97. Sahbeni, G. Prediction of Soil Salinity Using a Random Forest-Based Model between 2000 and 2016. A Case Study in the Great Hungarian Plain. In Proceedings of the Global Symposium on Salt-Affected Soils, online, 20–22 October 2021.
98. Hateffard, F.; Balog, K.; Tóth, T.; Mészáros, J.; Árvai, M.; Kovács, Z.A.; Szűcs-Vásárhelyi, N.; Koós, S.; László, P.; Novák, T.J.; et al. High-Resolution Mapping and Assessment of Salt-Affectedness on Arable Lands by the Combination of Ensemble Learning and Multivariate Geostatistics. *Agronomy* **2022**, *12*, 1858. [[CrossRef](#)]
99. Dajic-Stevanovic, Z.; Pecinar, I.; Kresovic, M.; Vrbnicanin, S.; Tomovic, L. Biodiversity, Utilization and Management of Grasslands of Salt Affected Soils in Serbia. *Community Ecol.* **2008**, *9*, 107–114. [[CrossRef](#)]
100. Szabolcs, I.; Rédly, M. State and Possibilities of Soil Salinization in Europe. *Agrokémia Talajt.* **1989**, *38*, 537–558.
101. Szabolcs, I.; Máté, F. A Hortobágyi Szikes Talajok Genetikájának Kérdéséhez. [On the Genesis of Alkaline Soils of Hortobágy]. *Agrokémia Talajt.* **1955**, *4*, 31–38.
102. Kovda, V.A. *Origin of Saline Soils and Their Regime I*; USSR Academy of Sciences: Moscow, Russia, 1946. (In Russian)
103. Kovda, V. *Origin of Saline Soils and Their Regime II*; USSR Academy of Sciences: Moscow, Russia, 1947. (In Russian)
104. Várallyay, G. Extreme Moisture Regime as the Main Limiting Factor of the Fertility of Salt Affected Soils. *Agrokémia Talajt.* **1981**, *30*, 73–96.
105. Wagenet, R.J.; Jury, W.A. Movement and Accumulation of Salts in Soils. In *Soil Salinity under Irrigation. Ecological Studies*; Shainberg, I., Shalhevet, J., Eds.; Springer: Berlin/Heidelberg, Germany, 1984; Volume 51, pp. 100–129.
106. Szabolcs, I.; Várallyay, G.; Darab, K. Soil and Hydrologic Surveys for the Prognosis and Monitoring of Salinity and Alkalinity. In Proceedings of the Prognosis of Salinity and Alkalinity. Report of an Expert Consultation, Rome, Italy, 3–6 June 1975; FAO Soil Bulletin 31. FAO: Rome, Italy, 1976; pp. 119–130.
107. Várallyay, G. Environmental Stresses Induced by Salinity/Alkalinity in the Carpathian Basin (Central Europe). *Agrokémia Talajt.* **2004**, *51*, 233–242. [[CrossRef](#)]
108. Dítě, Z.; Šuvada, R.; Tóth, T.; Jun, P.E.; Piš, V.; Dítě, D. Current Condition of Pannonic Salt Steppes at Their Distribution Limit: What Do Indicator Species Reveal about Habitat Quality? *Plants* **2021**, *10*, 530. [[CrossRef](#)]
109. Csontos, P.; Tamás, J.; Kovács, Z.; Schellenberger, J.; Penksza, K.; Szili-Kovács, T.; Kalapos, T. Vegetation Dynamics in a Loess Grassland: Plant Traits Indicate Stability Based on Species Presence, but Directional Change When Cover Is Considered. *Plants* **2022**, *11*, 763. [[CrossRef](#)] [[PubMed](#)]
110. Molnár, Z. Ősi És Másodlagos Eredetű Tiszántúli Szikes Puszták Zonációja [Zonation of Primary and Secondary Solonetz Alkaline Steppes in the Crisicum (Pannonicum)]. *Acta Biol. Debrecina. Suppl. Oecol. Hung.* **2010**, *22*, 181–189.
111. Kertész, M.; Tóth, T. Soil Survey Based on Sampling Scheme Adjusted to Local Heterogeneity. *Agrokémia Talajt.* **1994**, *43*, 113–132.
112. Steven, M.; Malthus, T.; Danson, F.; Jaggard, K.; Andrieu, B. Monitoring Response of Vegetation to Stress. In Proceedings of the Proceedings Remote Sensing Society Annual Conference, Dundee, UK, 15–17 September 1992; pp. 369–377.
113. Tóth, T. Salt-Affected Soils and Their Native Vegetation in Hungary. In *Sabkha Ecosystems: Volume III: Africa and Southern Europe*; Öztürk, M., Böer, B., Barth, H.-J., Clüsener-Godt, M., Khan, M.A., Breckle, S.-W., Eds.; Springer: Dordrecht, The Netherlands, 2011; pp. 113–132. ISBN 978-90-481-9673-9.

Disclaimer/Publisher’s Note: The statements, opinions and data contained in all publications are solely those of the individual author(s) and contributor(s) and not of MDPI and/or the editor(s). MDPI and/or the editor(s) disclaim responsibility for any injury to people or property resulting from any ideas, methods, instructions or products referred to in the content.